Available online at www.sciencedirect.com
ScienceDirect
Earth and Planetary Science Letters 260 (2007) 86–97
EPSL
www.elsevier.com/locate/epsl

Magnetic properties and geochemistry of the Xiashu Loess in the present subtropical area of China, and their implications for pedogenic intensity

Weiguo Zhang [a,*], Lizhong Yu [a], Min Lu [b], Xiangmin Zheng [b], Yuxin Shi [b]

[a] State Key Laboratory of Estuarine and Coastal Research, East China Normal University, Shanghai 200062, China
[b] Department of Geography, East China Normal University, Shanghai 200062, China

Received 20 November 2006; received in revised form 11 May 2007; accepted 11 May 2007
Available online 23 May 2007
Editor: M.L. Delaney

Abstract

Variations in the magnetic susceptibility of Chinese loess have been used to indicate pedogenic intensity and therefore past climate across the Chinese Loess Plateau (CLP). However, the relationship between climate and magnetic properties has not been fully resolved, and therefore a study of loess sections distributed over a wider climatic region is timely. In this study, we have investigated a 22.1 m loess section (named the Xiashu Loess) at Dagang, China, by integrating both rock magnetic and geochemical proxies. This loess profile is situated in a modern subtropical climate region with annual mean precipitation and temperature of 1100 mm and 15.4 °C, respectively, and therefore has experienced a stronger weathering intensity due to its lower latitude, higher temperature and rainfall. Geochemical and magnetic evidence indicate the same source area for the Xiashu Loess as for loess in northern China. The magnetic mineral assemblage of the Xiashu Loess is dominated by a higher concentration of superparamagnetic (SP)/single domain (SD) magnetite/maghemite grains in strongly weathered paleosols than in the loess layers, consistent with the production of fine-grained ferrimagnetic minerals during pedogenic processes. Nevertheless, compared to loess in the CLP, the Xiashu Loess shows: 1) reduced contrasts in magnetic susceptibility (χ), Hard Isothermal Remanent Magnetization (HIRM) and remanence of coercivity (B_{cr}) between loess and paleosols units, which indicates that the loess units have undergone stronger pedogenic alterations; 2) lower peak values of HIRM and χ in paleosols. In addition, the ratios SIRM/χ, χ_{ARM}/SIRM (where SIRM and χ_{ARM} are Saturation Isothermal Remanent Magnetization and the susceptibility of Anhysteretic Remanent Magnetization, respectively) and B_{cr} are found to be significantly correlated with the quotient (CaO*+Na_2O+MgO)/TiO_2, a geochemical indicator of pedogenic intensity. Overall, it seems that pedogenic processes in the Xiashu Loess lead to a relative increase in fine-grained ferrimagnetic SP/SD grains but depletion of anti-ferromagnetic minerals. Magnetic and geochemical proxies indicate strengthened East Asia summer monsoon during Marine Isotope Stages 13, 11 and 5, which is in good agreement with the records from the CLP and the South China Sea.

Keywords: magnetic properties; geochemistry; pedogenic intensity; loess; Xiashu Loess; China

1. Introduction

The thick wind-blown loess deposits in the Chinese Loess Plateau (CLP) have been regarded as one of the

* Corresponding author. Tel.: +86 21 62232482; fax: +86 21 62546441.
E-mail address: wgzhang@sklec.ecnu.edu.cn (W. Zhang).

0012-821X/$ - see front matter © 2007 Elsevier B.V. All rights reserved.
doi:10.1016/j.epsl.2007.05.018

best media to document global paleoclimatic changes (Liu, 1985; An, 2000). The fact that the mass specific magnetic susceptibility (χ) of the loess–paleosol sequences correlates well with the marine oxygen isotope record (Heller and Liu, 1984, 1986) has led to wide interest in the study of loess magnetism (Evans and Heller, 2001; Liu et al., 2007 and references therein). Despite the many successful applications of magnetic susceptibility in Chinese loess studies, there still exist problems with the paleoclimatic interpretation of magnetic proxies (Evans and Heller, 2001), as, for example, in the case of the quantitative relationship between χ and rainfall (Heller et al., 1993; Maher and Thompson, 1995). Magnetic investigations of loess sections spanning the climatic gradient across the loess plateau have been widely carried out, in order to better understand the climate-magnetism linkages in loess (e.g., Maher and Thompson, 1995; Guo et al., 2001). However, these studies have been concentrated on loess sections mostly in the arid and semi-arid temperate regions of China (e.g., Liu et al., 1999; Florindo et al., 1999; Deng et al., 2005).

To have a complete view of the magnetic responses to different climatic environments, this study investigated the Xiashu Loess distributed along the lower reach of the Yangtze River around Nanjing and Zhenjiang, presently a subtropical region with annual mean precipitation and temperature of 1100 mm and 15.4 °C, respectively (Li and Fang, 1993; Zheng, 1999) (Fig. 1). The Xiashu Loess has a provenance similar to the loess in northern China (Liu, 1985; Li and Fang, 1993; Zheng, 1999; Yang et al., 2004). Five major paleosols can be clearly identified in the Xiashu Loess sections, which can be correlated with the five soil units (S1–S5) in the upper part of loess in the CLP (Liu, 1985). It was therefore suggested that the Xiashu Loess was deposited since ~500 ka (Liu, 1985), which is close to the basal age of ~560 ka given by electron spin resonance dating (Li et al., 1993). This interval corresponds to a stage of strengthened East Asia winter monsoon (Xiao and An, 1999), which is also recorded in sediments of the South China Sea (Sun et al., 2003).

Except for some reports of magnetic susceptibility (Xia et al., 1999; Li et al., 2001), a multi-parameter magnetic characterization has never been carried out for the Xiashu Loess. In view of the geographical location of the Xiashu Loess, this work will complement magnetic studies in northern China and contribute to a better understanding of the relationship between loess magnetism and pedogenic intensity and hence paleoclimate.

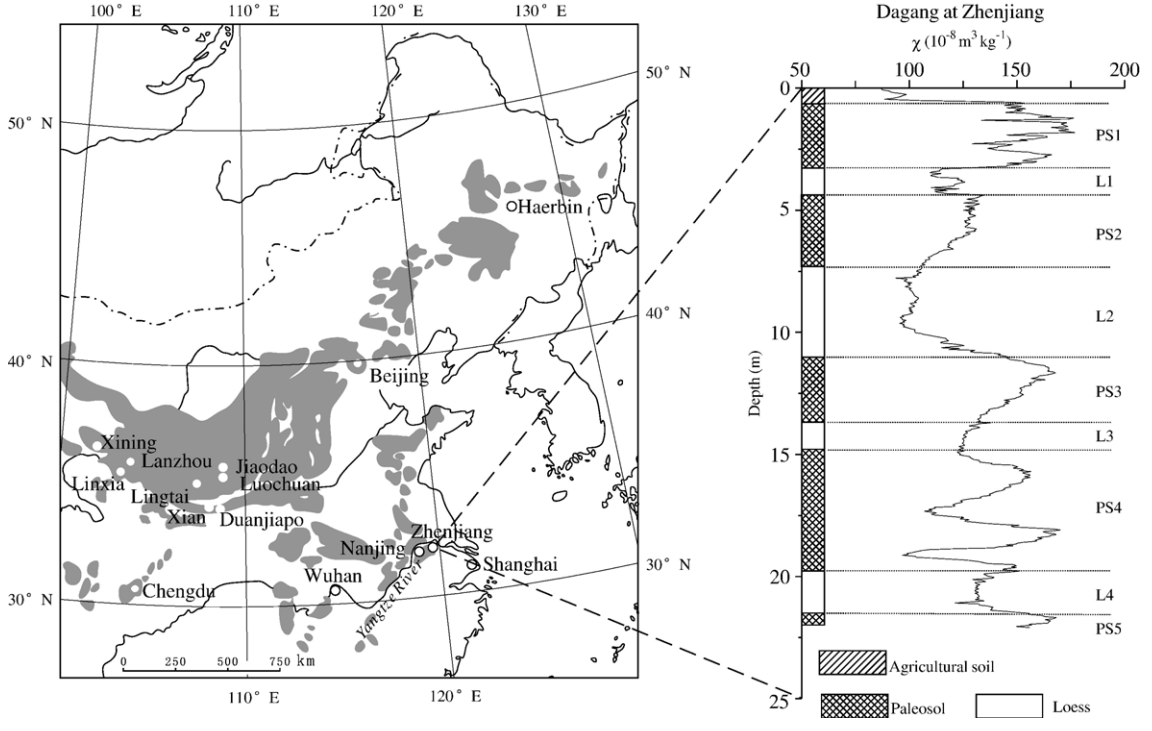

Fig. 1. Map showing the location of the Dagang section at Zhenjiang, the lower reach of the Yangtze River, and sites of other loess sections mentioned in this paper. The shaded area indicates the distribution of loess in China (Liu, 1985). The diagram on the right side shows the alternation of loess and paleosol units in the Dagang section.

To this end, geochemical proxies of chemical weathering are included to assist the paleoclimatic interpretation of the magnetic signals.

2. Samples and methods

2.1. Site description and samples

The Dagang section is located on the southern bank of the lower Yangtze River near Zhenjiang (Fig. 1). The section is 22.1 m in thickness, and it contains five paleosol units, which are named PS1, PS2, PS3, PS4 and PS5 from the top to the base (Fig. 1). The intervening loess layers are named L1, L2, L3 and L4 with increasing depth. Paleosols are compact, characterized by strong clayization and abundant iron/manganese coatings and roots. In contrast, loess units are generally yellowish in color, loose and porous. Field observations indicate that L2 is the coarsest loess layer. Above L2, paleosols PS1 and PS2 are dark brown in color, while the paleosols below L2 (PS3, PS4 and PS5) are characterized by a more reddish color. Paleomagnetic results show that the whole profile has been deposited during the Brunhes Normal Chron (Liu Huangfeng, personal communication), which is consistent with magnetostratigraphy studies on sections elsewhere in the Nanjing area (Fig. 1) (Huang et al., 1988; Qiao et al., 2003). Stratigraphic and magnetic correlation with the optical stimulated luminescence dated loess section at Nanjing (Xia et al., 1999; Lai et al., 2001), suggest that PS1 was formed during Marine Isotope Stage 5 (MIS 5). The basal age of this section is estimated as around 500 ka (Liu, 1985). The section was sampled at 4 cm intervals, which resulted in a total of 552 samples. The samples were dried at a low temperature of 40 °C and disaggregated before analyses.

2.2. Magnetic measurements

Magnetic susceptibility, Isothermal Remanent Magnetization (IRM) after applying a field of 1 T, and then back field remanence measurements at −20 mT, −40 mT, −100 mT and −300 mT were first measured on all samples. The corresponding IRM is referred to IRM_{xmT}, where the subscript *x*mT indicates the field value. Selected samples (~40 cm interval) were then subjected to measurements of Anhysteretic Remanent Magnetization (ARM), hysteretic loops and thermomagnetic curves. Both low (0.47 kHz) and high (4.7 kHz) frequency susceptibilities (χ_{lf} and χ_{hf}, respectively) were measured with a Bartington MS2B meter. Frequency dependent susceptibility (χ_{fd}) was calculated as $\chi_{fd}=(\chi_{lf}-\chi_{hf})$. χ_{fd}% was obtained by expressing χ_{fd} as a percentage of χ_{lf}. In this study, IRM obtained at 1 T was referred to as SIRM. Hard IRM (HIRM) was defined as $HIRM=0.5\times(SIRM+IRM_{-300\ mT})$. S_{-100} and S_{-300} were calculated as $S_{-100}=IRM_{-100\ mT}/SIRM$ and $S_{-300}=IRM_{-300\ mT}/SIRM$, respectively. ARM was acquired in a 0.04 mT DC field superimposed on a peak AF demagnetization field of 100 mT, and expressed as susceptibility of ARM (χ_{ARM}). Both the IRMs and ARM were measured using a Molspin magnetometer. Hysteresis loops were measured using a Variable Field Translational Balance (VFTB) with a maximum field of ±1 T. Saturation magnetization (M_s), Saturation remanence (M_{rs}), and coercivity (B_c) were determined after subtraction for a paramagnetic contribution. Paramagnetic susceptibility (χ_p) was then derived from the high-field slope of the hysteresis loops (between 0.7 T and 1 T). Ferrimagnetic susceptibility (χ_f) was defined as the difference between χ_{lf} and χ_p. Coercivity of remanence (B_{cr}) was obtained by SIRM demagnetization using the VFTB. Magnetization versus temperature curves were obtained with the VFTB in air using a field of 420 mT.

In addition, selected samples taken at ~40 cm intervals were treated with a citrate–bicarbonate–dithionite (CBD) extraction procedure (Mehra and Jackson, 1958), which is effective at removing fine-grained pedogenic ferrimagnetic minerals (Verosub et al., 1993). The method is described in detail by Vidic et al. (2000). After a total reaction time of 30 mins, the solid residues were then dried at 40 °C for magnetic susceptibility and SIRM measurements.

2.3. Geochemical and granulometric characterization

The selected samples (~40 cm intervals) were also subjected to geochemical and granulometric characterization. Major elements and Rb, Sr and Ba concentrations were determined with an ARL9800 XP+X-ray fluorescence spectrometer. Analytical uncertainties are within 5% for all elements. The Chemical Index of Alteration (CIA) was calculated as $CIA=[Al_2O_3/(Al_2O_3+CaO^*+Na_2O+K_2O)]\times 100$ (molar ratio), where CaO* represents the amount of CaO in the silicate fraction of the sample (Nesbitt and Young, 1982). CIA and Rb/Sr are commonly used as indicators of pedogenic intensity (Liu, 1985; Jahn et al., 2001), with higher values corresponding to stronger chemical weathering. The quotient $(CaO^*+Na_2O+MgO)/TiO_2$, a proxy proposed by Yang et al. (2006) as being independent of particle size, has also been calculated. In contrast to the above geochemical proxies, this ratio and

Na_2O/Al_2O_3 decrease with increased degree of pedogenesis (Yang et al., 2006). Particle size was analyzed with a laser size analyzer (Coulter LQ-100Q).

3. Results

The depth variations of bulk magnetic properties are presented in Fig. 2. They clearly divide the samples into two groups (Figs. 3 and 4, Table 1). Group 1 includes samples from units L1, PS2, L2, PS3, L3 and L4. The samples within paleosols PS1, PS4 and PS5 form Group 2. Geochemical and granulometric data (Fig. 5) are used to constrain the mechanism of the differences in magnetic properties of the two groups.

3.1. Concentration related magnetic parameters

The values of χ (here refers to χ_{lf}) vary from 87×10^{-8} m^3 kg^{-1} to 177×10^{-8} m^3 kg^{-1} (Fig. 2a). The paramagnetic susceptibility (χ_p) ranges between 4.7×10^{-8} m^3 kg^{-1} and 9.2×10^{-8} m^3 kg^{-1}, accounting for 4.3%–8.6% of the bulk χ. In general, paleosols show higher χ values than the neighboring loess layers (Fig. 2a). However, strong fluctuations of χ within paleosol PS4 are observed, with the lowest value comparable to those of loess L2.

SIRM is generally used as an approximation of total magnetic mineral concentration with grain size larger than the superparamagnetic (SP)/single domain (SD) threshold. Unlike χ, SIRM is not influenced by (super) para- and dia-magnetic minerals (Thompson and Oldfield, 1986). It has a pattern not completely in agreement with that of χ (Fig. 2b). On the plot of SIRM versus χ, the samples can be clearly divided into two groups (Fig. 3a).

χ_{fd} reflects the presence of fine viscous grains close to the SP/SD boundary (~0.02 μm) (Thompson and Oldfield, 1986), while χ_{ARM} is sensitive to single domain (SD, ~0.02–0.06 μm) grains (Maher, 1988).

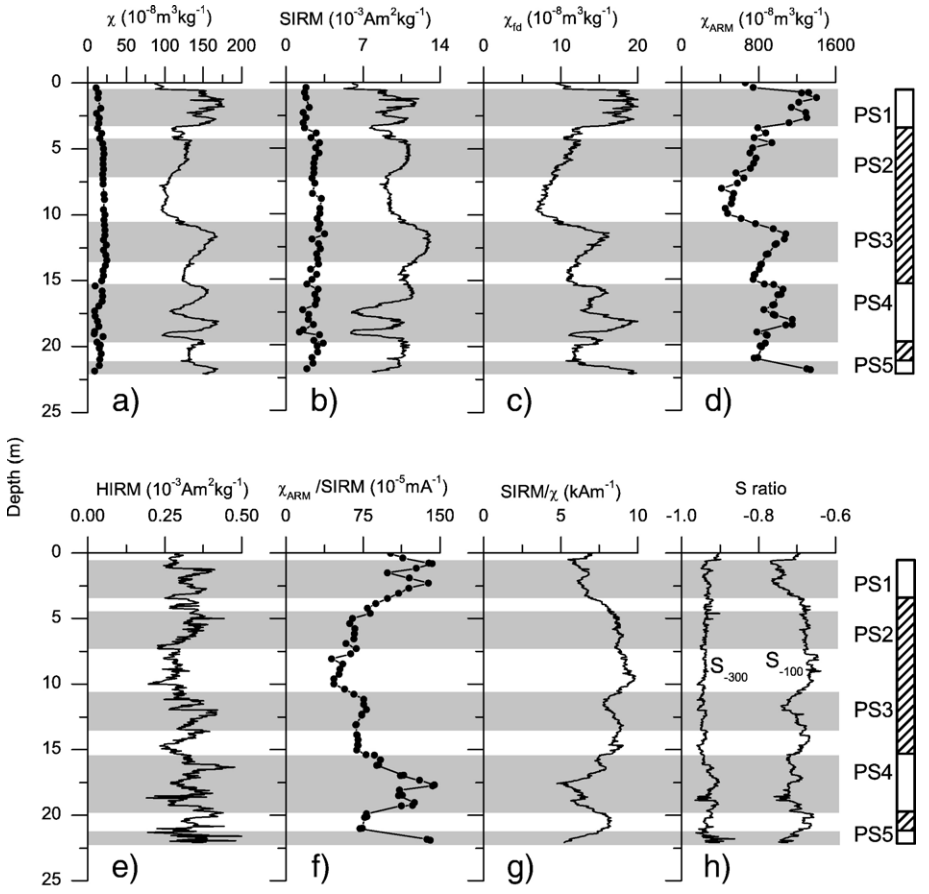

Fig. 2. Magnetic properties for the Dagang section. Dotted lines in (a) and (b) indicate χ and SIRM after the CBD treatment. The shaded zones indicate paleosol units. The line fill pattern and blank part of the bar on the right side denote Groups 1 and 2, respectively.

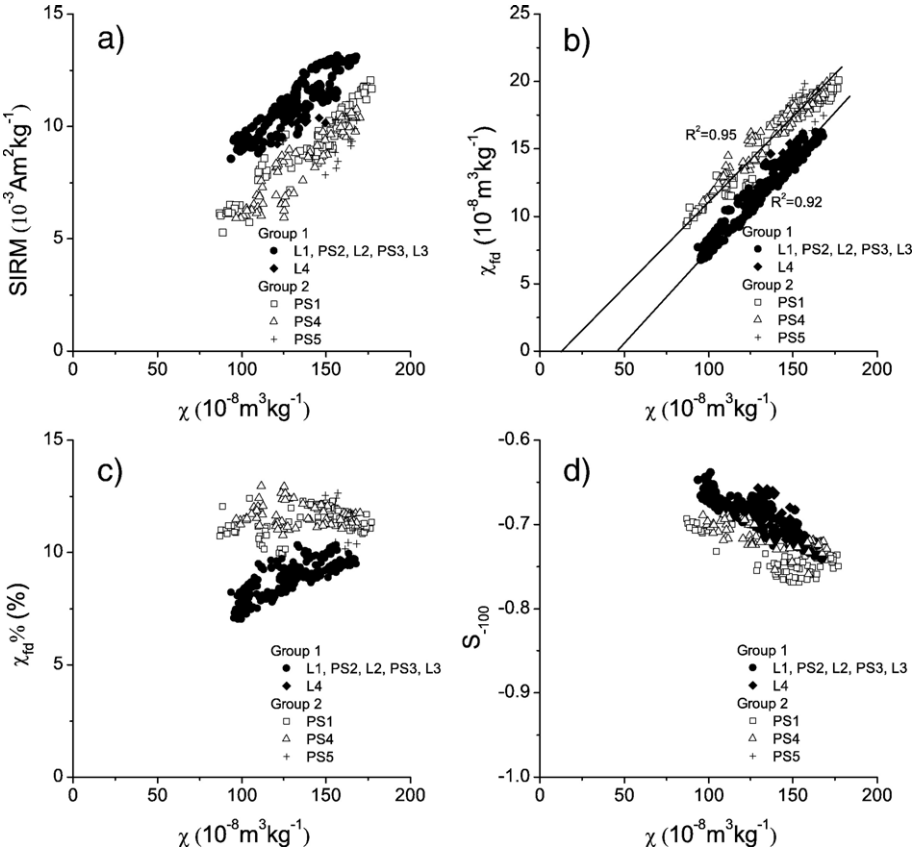

Fig. 3. Variations of (a) SIRM, (b) χ_{fd}, (c) χ_{fd}% and (d) S–sub $_{100}$ versus χ. Two groups of samples can be clearly identified, with samples from PS2, PS3, and loess layers L1, L2, L3 and L4 (Group 1) different from those of paleosols PS1, PS4 and PS5 (Group 2). The intercepts of χ_{fd} versus χ correlation lines with the x-axis in (b) are 45×10^{-8} m^3 kg^{-1} and 12×10^{-8} m^3 kg^{-1} for Groups 1 and 2, respectively.

They co-vary with each other and show similar depth-variations with that of χ (Fig. 2c–d), indicating that χ is influenced by both SP and SD grains. A linear relationship between χ_{fd} and χ is found for both groups with similar slopes of the regression lines (Fig. 3b).

HIRM provides a rough estimate of the concentration of anti-ferromagnetic minerals (Bloemendal and Liu, 2005). Although it varies with loess–paleosol alternations (Fig. 2e), with higher values in paleosols and lower values in loess layers, the amplitude of fluctuation is much reduced compared to χ and SIRM.

3.2. Magnetic grain size

χ_{fd}% is an estimation of the relative contribution of fine viscous SP grains to the total magnetic assemblage (Thompson and Oldfield, 1986). It ranges from 7% to 13%, with higher values in Group 2 samples (see Fig. 1a in the Appendix). Accordingly, samples with higher χ_{fd} % values display lower SIRM/χ ratios (Fig. 2g). χ_{fd}% is positively correlated with χ for Group 1 samples, while it shows almost no correlation with χ for Group 2 samples (Fig. 3c).

χ_{ARM}/SIRM is commonly used as a grain size indicator of ferrimagnetic minerals, which peaks in SD range and decrease with increasing grain size (Maher, 1988). Its profile is similar to that of χ_{fd}% (Fig. 2f), and it suggests that the magnetic minerals in Group 2 samples are relatively finer than in Group 1 samples. χ_{ARM}/χ_f is also a convential grain size proxy (Banerjee et al., 1981). It displays similar variations with χ_{ARM}/SIRM (see Fig. 1c in the Appendix), but with a smaller fluctuation amplitude, which points to the reduction of χ_{ARM}/χ_f ratios due to the greater contribution of SP grains in Group 2 samples.

On a plot of M_{rs}/M_s versus B_{cr}/B_c, all samples fall in the pseudo-single-domain (PSD) region of Day plot (Day et al., 1977), with Group 2 samples more close to the SD region (Fig. 4). Considering significant χ_{fd}% and χ_{ARM}/SIRM values of the samples and the wasp-waisted

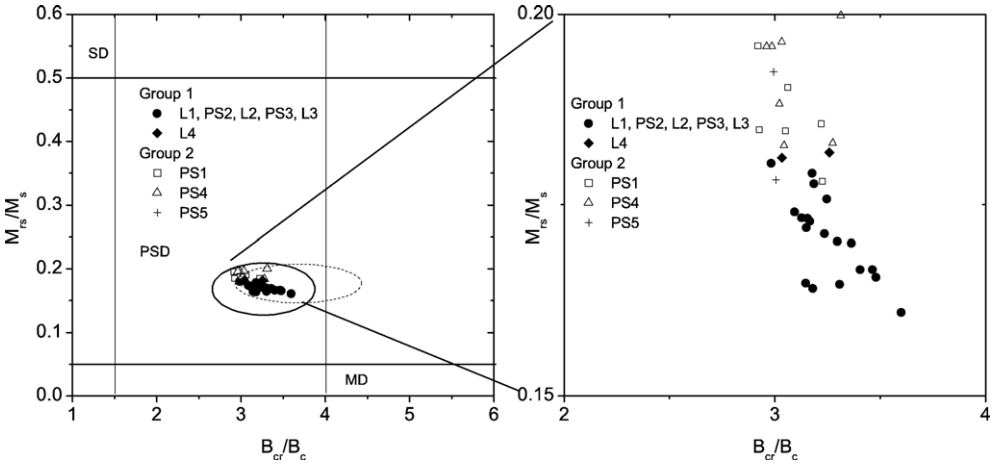

Fig. 4. Hysteresis ratios plotted on a Day diagram (Day et al., 1977). Samples from Group 1 are closer toward SD region, indicating a finer grain size. The solid and dashed circles depict the position of samples from Luochuan (Fukuma and Torri, 1998) and Duanjiapo (Florindo et al., 1999), respectively.

forms of the loops (see Fig. 2 in the Appendix), it largely reflects the fact of a mixture of multi-domain (MD) and SD/SP sizes (Tauxe et al., 1996; Dunlop, 2002).

3.3. Magnetic mineralogy

It is found that SIRM of all samples is demagnetized in backfields ranging between −20 mT and −40 mT and detailed demagnetization curves on selected samples reveal B_{cr} values between 20 mT and 33 mT (see Fig. 1d in the Appendix), suggesting a dominance of the magnetic properties by low coercivity ferrimagnetic minerals.

S_{-300} serves as a measure of the relative importance of higher coercivity minerals (i.e., hematite and goethite) and lower coercivity components (i.e., magnetite and maghemite) in the total assemblage (Bloemendal and Liu, 2005). Most of the samples have S_{-300} lower

Table 1
Summary of magnetic properties and geochemical pedogenic intensity indicators for the two groups of the Xiashu Loess, and their comparisons with Luochuan section in northern China

	Group 1 (L1, PS2, L2, PS3, L3 and L4)			Group 2 (PS1, PS4 and PS5)			Luochuan section[a] (S0–S5)		
	Minimum	Maximum	Mean±SD	Minimum	Maximum	Mean±SD	Minimum	Maximum	Mean±SD
χ (10^{-8} m^3 kg^{-1})	94	168	128±18	87	177	139±24	23	277	106±63
SIRM (10^{-3} Am^2 kg^{-1})	8.6	13.1	10.8±1.1	5.3	12.1	8.8±1.6	4.7	19.9	10.0±3.8
χ_{fd} (10^{-8} m^3 kg^{-1})	6.8	16.2	11.4±2.5	9.4	20.3	16.0±2.9	0.9	31.6	9.3±7.2
χ_{ARM} (10^{-8} m^3 kg^{-1})	416	1085	786±164	745	1402	1046±208	100	1909	611±437
HIRM (10^{-3} Am^2 kg^{-1})	0.20	0.53	0.32±0.05	0.15	0.48	0.34±0.05	0.17	0.90	0.43±0.10
χ_{fd}% (%)	7.0	10.7	8.8±0.8	10.0	13.0	11.5±0.6	2.6	11.6	7.9±1.9
χ_{ARM}/SIRM (10^{-5} m A^{-1})	44.5	92.7	69.7±12.1	87.3	144.2	119.0±14.9	19.8	98.8	54.4±19.2
χ_{ARM}/χ	4.2	7.4	6.1±0.7	6.8	8.7	7.7±0.5	3.5	7.0	5.4±0.8
SIRM/χ (kA m^{-1})	6.8	9.9	8.5±0.6	4.7	7.7	6.3±0.5	6.8	21.3	10.7±2.6
S_{-100} (%)	−0.74	−0.64	−0.69±0.02	−0.77	−0.68	−0.72±0.02	−0.78	−0.30	−0.58±0.11
S_{-300} (%)	−0.98	−0.90	−0.94±0.01	−0.96	−0.86	−0.93±0.01	−0.97	−0.67	−0.91±0.03
B_{cr} (mT)	22.8	32.9	28.2±2.6	20.7	25.9	23.0±2.0			
χ_0 (10^{-8} m^3 kg^{-1})	45			12			18		
CIA	63.9	71.0	66.5±1.9	65.4	73.7	70.3±1.9			
Rb/Sr	0.78	1.08	0.91±0.08	0.80	1.20	1.06±0.09			
$(CaO^*+Na_2O+MgO)/TiO_2$	6.1	8.1	7.2±0.5	4.9	6.4	5.7±0.4			

[a] The data for Luochuan section are derived from (Bloemendal and Liu, 2005) and calculated only for the period of last 500 ka for comparative purpose.

than −0.9 (Fig. 2h), confirming the predominance of ferrimagnetic contributions to the magnetic properties. S_{-100} also reflects the mineral assemblage variation of samples, but can be influenced by grain size variations in ferrimagnetic minerals, with SD grains having higher coercivities than MD grains (Robinson and Sahota, 2000). S_{-100} displays an opposite trend to that of χ_{ARM} and χ_{ARM}/SIRM (Fig. 2), implying that higher S_{-100} values are not caused by a higher proportion of SD grains. Therefore S_{-100} is mainly controlled by the varying proportions of ferrimagnetic versus canted antiferromagnetic minerals (Robinson and Sahota, 2000), with a relatively lower contribution of canted antiferromagnetic minerals in Group 2 samples (Fig. 3d).

Both paleosols and loess samples display Curie temperatures around 600 °C and an inflection between 300 °C and 550 °C on the heating curves (see Fig. 3 in the Appendix), suggesting that partially maghemitised magnetite (Eyre and Shaw, 1994; Liu et al., 1999) dominates magnetic properties of the Xiashu Loess.

3.4. Influence of CBD extraction on χ and SIRM

It is well established that magnetic minerals in loess can be divided into detrital and pedogenic components (Zhou et al., 1990; Zheng et al., 1991; Maher and Thompson, 1991; Banerjee et al., 1993; Verosub et al., 1993; Heller et al., 1993). The CBD extraction method selectively removes the fine-grained pedogenic magnetic minerals, with the post-CBD value of χ providing first approximation of the contribution from the detrital component (Verosub et al., 1993; Hunt et al., 1995). After CBD extraction, the post-CBD χ varies between 7×10^{-8} m^3 kg^{-1} and 23×10^{-8} m^3 kg^{-1} (Fig. 2a), which accounts for only 7–22% of the original susceptibility. On average, Group 1 samples show higher post-CBD χ and SIRM values (19×10^{-8} m^3 kg^{-1}, 2.8×10^{-3} Am^2 kg^{-1}, respectively) than Group 2 samples (12×10^{-8} m^3 kg^{-1}, 1.9×10^{-3} Am^2 kg^{-1}, respectively) (Fig. 2a–b).

3.5. Geochemical characterization and particle size composition

Depth variations of major and trace elements are illustrated in Fig. 4 in the Appendix. Most of the elements display rather small variations, with the coefficients of variations (CV) less than 5%. The contents of CaO, Na_2O, P_2O_5 and Sr exhibit slight stronger variations, with lower values occurring in Group 2 samples. Nevertheless, the CVs of these elements are less than 15%. It suggests that the Xiashu Loess has a relatively stable source area. The vertical variations of these elements are consistent with the fact that chemical weathering has led to the removal of easily mobile elements like Ca, Na, P and Mg, and the enrichment of immobile elements like Al, Fe and Ti in paleosols (Jahn et al., 2001; Yang et al., 2006). As expected, the values of pedogenic indicators used in loess studies, such as CIA and Rb/Sr are higher in Group 2 samples (Fig. 5a–b), while the quotients ($CaO^*+Na_2O+MgO)/TiO_2$ and Na_2O/Al_2O_3 show the opposite trend (Fig. 5c–d), suggesting a stronger pedogenic intensity within these units. The Xiashu Loess is rather uniform in particle size composition (Fig. 5e), implying that particle size plays a minor role in the variations of element contents and pedogenic proxies.

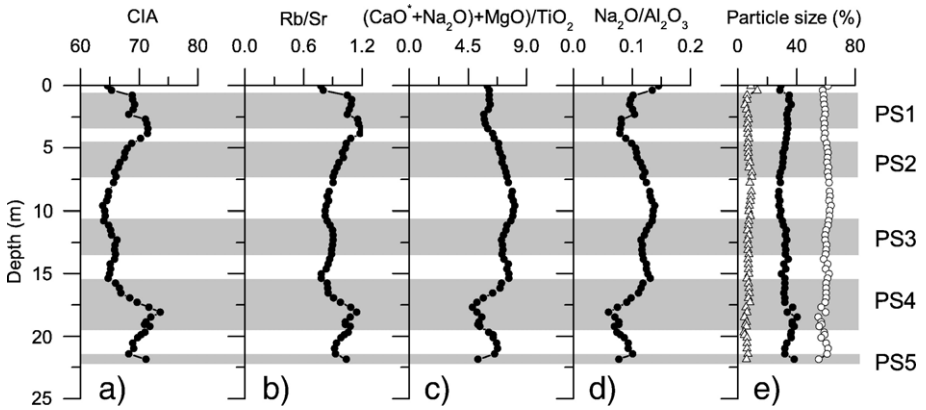

Fig. 5. Variations of (a–d) geochemical proxies of pedogenic intensity and (e) particle size compositions in the Dagang section. The shaded zones indicate paleosol units. Closed dot, open dot and open triangle in (e) represent the fractions of clay (<5 μm), silt (5–50 μm) and sand (>50 μm), respectively.

3.6. Summary of magnetic and geochemical properties of the two groups

In summary, Group 2 samples show higher concentrations of finer ferrimagnetic minerals and increased proportions of ferrimagnetic minerals to canted antiferromagnetic minerals. Group 1 samples are characterized by coarser ferrimagnetic grain size. The geochemical pedogenic proxies indicate a stronger degree of chemical weathering experienced by the Group 2 samples (Table 1).

4. Discussion

4.1. Magnetic minerals and the influence of pedogenesis

The above results demonstrate that magnetite and maghemite dominate the magnetic properties of the Xiashu Loess. The most striking differences in magnetic properties lie in the distinction of two group samples, with Group 2 exhibiting a greater amount of SP/SD grains. It is worth noticing that paleosols PS2 and PS3 are magnetically grouped with loess layers L1, L2, L3 and L4. It demonstrates that the terms 'loess' and 'paleosol' only have relative meanings. Considering the homogeneity in geochemical and particle size compositions (Fig. 5), higher SP/SD grains in Group 2 samples are mainly produced during periods of intensified pedogenesis, which is in consistence with magnetic enhancement observed in loess sections from northern China (Zhou et al., 1990; Zheng et al., 1991; Maher and Thompson, 1991; Banerjee et al., 1993; Verosub et al., 1993). The higher concentration of detrital coarse-grained magnetic minerals in Group 1 samples could be caused by stronger winter monsoon and/or shorter distances from the source area during periods of weaker pedogenesis (Deng et al., 2005).

Pronounced rubification of paleosols PS3, PS4 and PS5 is suggestive of the presence of hematite (Cornell and Schwertmann, 2003). Furthermore, previous heavy mineral analysis has clearly reported the presence of hematite in the Xiashu Loess (Zheng, 1999). Compared to χ_{fd} and χ_{ARM}, the smaller increase of HIRM values in paleosols suggests the greater relative importance of ferrimagnetic minerals in the pedogenic magnetic enhancement process (Zheng et al., 1991).

4.2. Magnetic comparison with loess in northern China

The Xiashu Loess shows great similarity in major element compositions to those of Lingtai section in the CLP (Fig. 6a), confirming that it has a provenance similar to that of the loess in northern China (Liu, 1985; Li and Fang, 1993; Zheng, 1999; Yang et al., 2004). Although the bulk magnetic susceptibility varies across the CLP, both spatially and temporally, χ of detrital component has been found to be relatively stable (Verosub et al., 1993; Forster et al., 1994). The post-CBD χ values of the Xiashu loess ($7–23\times10^{-8}$ m^3 kg^{-1}) are quite close to the values previously reported for loess from the CLP, e.g., $15\pm4\times10^{-8}$ m^3 kg^{-1} from Luochuan (Verosub et al., 1993), $7–28\times10^{-8}$ m^3 kg^{-1} from Jiaodao (Deng et al., 2005).

Liu et al. (2004) used 'corrected χ_{fd}%', or 'true F factor' named by Forster et al. (1994), to assess the grain size distribution of pedogenic ferrimagnetic minerals. The corrected χ_{fd}% is calculated as $\chi_{fd}/(\chi-\chi_0)\times100$, where χ_0 represents the background susceptibility of detrital component (Forster et al., 1994; Liu et al., 2004). In Fig. 3b, the value of χ where χ_{fd} is zero (the intercept with the *x*-axis) refers to χ_0. The χ_0 value for Group 2 (12×10^{-8} m^3 kg^{-1}) matches well with the value estimated by DCB extraction. However, the χ_0 value for Group 1 (45×10^{-8} m^3 kg^{-1}) is clearly much higher than the post-CBD χ value. Considering the homogeneity in chemical composition throughout the section, it might indicate an additional source with a minor contribution but a stronger magnetic signal for Group 1. The CBD procedure probably can dissolve part of this detrital component (Vidic et al., 2000) and results in a lower post-CBD χ value for Group 2. The mechanism requires further study. The corrected χ_{fd}% values for Group 1 (~13.7%) and 2 (~12.6%) are closer to those of Yuanbao (~14%) and Jiaodao (12%) sections in the CLP (Vidic et al., 2000; Liu et al., 2004). The almost similar corrected χ_{fd}% values suggests that, in terms of magnetic minerals, the Xiashu Loess has experienced pedogenic environments similar to those affecting loess sections in northern China. On the Day plot, our samples fall in virtually the same position as those from Luochuan (Fukuma and Torri, 1998) and Duanjiapo (Florindo et al., 1999) in the CLP.

The minimum χ value (87×10^{-8} m^3 kg^{-1}) of the Xiashu Loess (Fig. 2a) is higher than the lowest values of loess samples ($21–27\times10^{-8}$ m^3 kg^{-1}) from sections in northern China (Maher and Thompson, 1991; Hunt et al., 1995; Florindo et al., 1999; Mishima et al., 2001). It suggests that the loess layers in the Xiashu Loess have experienced stronger weathering than their counterparts in northern China. If the present atmospheric circulation patterns remained the same during the past 600 ka (Hao and Guo, 2005), this is in accordance with the fact that Xiashu Loess is located at the warmest and wettest end along the NW–SE gradient of monsoon climate.

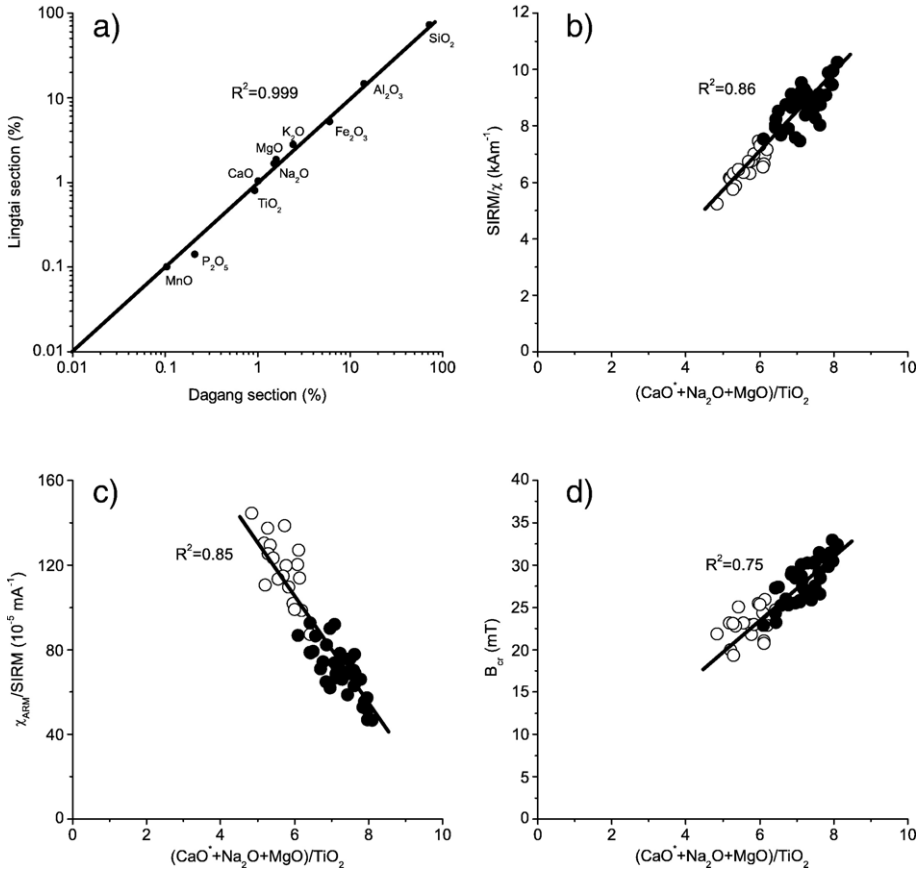

Fig. 6. (a) Comparison of the mean concentrations of major elements between the Dagang section and the Lingtai section (Yang et al., 2006) in northern China. Note that the samples from Lingtai were analyzed with carbonate removal pretreatment, while those of the Xiashu Loess are without such treatment, as carbonate is barely present. For the Xiashu Loess, the ratio $(CaO^{*}+Na_2O+MgO)/TiO_2$, an indicator of pedogenic intensity, is significantly correlated with magnetic parameters (b) SIRM/χ, (c) χ_{ARM}/SIRM and (d) B_{cr}. Closed and open dots represent Group 1 and Group 2 samples, respectively.

However, the maximum χ value of 177×10^{-8} m^3 kg^{-1} in the Xiashu Loess is lower than the value of 264×10^{-8} m^3 kg^{-1} reported for Duanjiapo section (Florindo et al., 1999) and other sites (Bloemendal and Liu, 2005), implying a non-linear relationship between χ and climate.

Similarly, the maximum HIRM value in the Xiashu Loess (0.48×10^{-3} Am^2 kg^{-1}) are comparatively lower than those of the Duanjiapo (1.13×10^{-3} Am^2 kg^{-1}) and Luochuan (0.90×10^{-3} Am^2 kg^{-1}) sections for the last 500 ka (Bloemendal and Liu, 2005). It suggests less favorable conditions for the production/preservation of anti-ferromagnetic minerals in the paleosols of the Xiashu Loess.

In the Xiashu Loess, paleosols show similar B_{cr} values with their counterparts in the CLP, but the loess layers display much lower B_{cr} values (no more than 33 mT). For example, B_{cr} values are 19–49 mT for paleosol S1 and loess L2 of the Duanjiapo section (Florindo et al., 1999). As the much weathered loess layers in the Xiashu Loess show enhanced χ but similar HIRM values to that of the Duanjiapo section ($\sim0.20\times10^{-3}$ Am^2 kg^{-1}, Bloemendal and Liu, 2005), the reduced B_{cr} values are caused by a rise in the proportion of ferrimagnetic minerals to anti-ferromagnetic minerals.

4.3. Proxy of pedogenic intensity

Magnetic susceptibility has been long used as a proxy of pedogenic intensity and hence climate (see reviews by Evans and Heller, 2001), although a number studies have called for its caution use in quantitative climatic reconstructions (e.g., Guo et al., 2001; Bloemendal and Liu, 2005). Our data indicates that χ alone cannot reflect the pedogenic strength faithfully. For example, within paleosol PS4, samples showing higher SP/SD grains are

characterized by lower χ values, which are even lower than those in the loess layers.

Loess deposition and pedogenesis are competing processes in loess, and what distinguishes loess from paleosol is their relative strengths as the climate fluctuates with time (Zheng et al., 1991; Verosub et al., 1993). Since ferrimagnetic minerals produced during pedogenesis are mainly fine-grained SP/SD particles, while detrital magnetic minerals have a relative coarser size, the grain size variation of magnetic minerals, which can be assessed by χ_{fd}%, χ_{ARM}/χ and χ_{ARM}/SIRM, may provide better paleoclimatic information (Geiss et al., 2004). In the present study, magnetic parameters SIRM/χ, χ_{ARM}/SIRM and B_{cr} seem to be the best indicators of pedogenic intensity (Fig. 6b–d). With increased degree of pedogenesis, the decrease in SIRM/χ and increase in χ_{ARM}/SIRM can be explained by increased contribution of fine-grained SP/SD ferrimagnetic grains. The decreased B_{cr} values in strongly weathered loess are consistent with the suggestion that, in soil forming processes, when the climatic threshold for peak production of anti-ferromagnetic minerals is passed, the proportion of pedogenic ferrimagnetic minerals will increase over antiferromagnetic minerals with increased rainfall and temperature, until the production and preservation of the former reach a maximum value (Balsam et al., 2004). Detailed study of magnetic grain size and mineralogy variations in response to rainfall and temperature will contribute to better quantitative climate reconstructions.

4.4. Implications for paleoclimate reconstruction

Magnetic and geochemical proxies indicate that the paleosols PS5, PS4 and PS1 represent the most developed soils in the Xiashu Loess. The paleosols correspond to periods of diminished dust deposition and enhanced soil formation, when the regional climate was dominated by stronger summer monsoon (Liu, 1985; Zheng et al., 1991; Verosub et al., 1993). They therefore indicate three periods with particularly strengthened summer monsoon. Such a temporal variations in East Asia summer monsoon intensity correlates well with the record from loess–paleosol sequences in the CLP, where the S5-1, S4 and S1 soils (corresponding to MIS 13, 11 and 5, respectively) are the strongest developed soils over the last 500 ka (Guo et al., 2000). Intensified summer monsoons during MIS 13, 11 and 5 are also clearly evident in the record from the South China Sea (Wei et al., 2003). Such a correspondence confirms previous stratigraphic correlation between the Xiashu Loess and loess sections in the CLP (Liu, 1985), and paleosols PS5, PS4, PS3, PS2 and PS1 are formed in MIS 13, 11, 9, 7 and 5, respectively. There is a weakening trend of summer monsoon from PS4 toward the lower part of L2, after which the trend is reversed. It seems that PS2 is by far the weakest soil, which also finds its counterpart during MIS 7 in the marine record (Wei et al., 2003). The variations in summer monsoon intensity recorded in the Xiashu Loess therefore is not a local feature, but is consistent with the regional climate fluctuations in East Asia.

5. Conclusions

In the Xiashu Loess along the lower reach of Yangtze River, a region characterized by a presently subtropical climate, magnetic and geochemical data clearly divided the samples into two groups, with the group exposed to stronger pedogenic processes containing higher proportions of SP/SD magnetite/maghemite. Previous suggestions that the Xiashu Loess has the same provenance as loess in northern China, are supported by their strong similarities in major element abundances and post-CBD susceptibility values. The Xiashu Loess also experienced a similar pedogenic environment as evidenced by its similar grain size distribution of pedogenic ferrimagnetic particles to that found in loess in northern China. In comparison to their counterparts in loess sections in northern China, the loess layers of the Xiashu Loess have higher χ and lower B_{cr} values, but the strongly weathered paleosols have lower values of χ and HIRM. Assuming that the pattern of past climatic conditions was similar to that prevailing at present, and bearing in mind that the Xiashu Loess is located at the warm and wet end of NW–SE gradient of Asian monsoon climate, this latter feature is interpreted as reflecting stronger weathering intensity and preferred generation of ferrimagnetic particles over hematite only up to the point at which further increases in temperature and precipitation no longer lead to increases in pedogenic ferrimagnets. SIRM/χ, χ_{ARM}/SIRM and B_{cr} are found to be the best indicators of pedogenic intensity in the study area, with lowered SIRM/χ and B_{cr}, but enhanced χ_{ARM}/SIRM values reflecting an increasing degree of pedogenesis. These new proxies indicate strengthened East Asia summer monsoon during MIS 13, 11 and 5, which is in good agreement with the records from the Chinese Loess Plateau and the South China Sea.

Acknowledgements

We thank F. Oldfield, Qingsong Liu and Zhongping Lai for their valuable comments and language improvements

on an earlier draft of this manuscript. Sincere thanks to C. P. Geiss and two anonymous reviewers for their critical comments, and J. Bloemendal for providing magnetic data for the Duanjiapo and Luochuan sections. This study was supported by National Natural Science Foundation of China (Grant No. 40001020).

Appendix A. Supplementary data

Supplementary data associated with this article can be found, in the online version, at doi:10.1016/j.epsl.2007.05.018.

References

An, Z.S., 2000. The history and variability of the East Asian paleomonsoon climate. Quat. Sci. Rev. 19, 171–187.

Balsam, W., Ji, J.F., Chen, J., 2004. Climatic interpretation of the Luochuan and Lingtai loess sections, China, based on changing iron oxide mineralogy and magnetic susceptibility. Earth Planet. Sci. Lett. 223, 335–348.

Banerjee, S.K., King, J., Marvin, J., 1981. A rapid method for magnetic granulometry with applications to environmental studies. Geophys. Res. Lett. 8, 333–336.

Banerjee, S.K., Hunt, C.P., Liu, X.M., 1993. Separation of local signals from regional paleomonsoon record of the Chinese Loess Plateau: a rock-magnetic approach. Geophys. Res. Lett. 20, 843–846.

Bloemendal, J., Liu, X.M., 2005. Rock magnetism and geochemistry of two Plio–Pleistocene Chinese loess–palaeosol sequences—implications for quantitative palaeoprecipitation reconstruction. Palaeogeogr. Palaeoclimatol. Palaeoecol. 226, 149–166.

Cornell, R.M., Schwertmann, U., 2003. The Iron Oxides: Structure, Properties, Reactions, Occurrences and Uses. Wiely-VCH Verlag GmbH & Co. KGaA, Weinheim.

Day, R., Fuller, M., Schmidt, V.A., 1977. Hysteresis properties of titanomagnetites: grain size and compositional dependence. Phys. Earth Planet. Inter. 13, 260–267.

Deng, C.L., Vidic, N.J., Verosub, K.L., Singer, M.J., Liu, Q.S., Shaw, J., Zhu, R.X., 2005. Mineral magnetic variation of the Jiaodao Chinese loess/paleosol sequence and its bearing on long-term climatic variability. J. Geophys. Res. 110, B03103. doi:10.1029/2004JB003451.

Dunlop, D.J., 2002. Theory and application of the Day plot (Mrs/Ms vs. Hcr/Hc) 2. Application to data for rocks, sediments and soils. J. Geophys. Res. 107B. doi:10.1029/ 2001JB000487.

Evans, M.E., Heller, F., 2001. Magnetism of loess/paleosol sequences: recent developments. Earth-Sci. Rev. 54, 129–144.

Eyre, J.K., Shaw, J., 1994. Magnetic enhancement of Chinese loess—the role of γFe_2O_3? Geophys. J. Int. 117, 265–271.

Florindo, F., Zhu, R.X., Guo, B., Yue, L.P., Pan, Y.X., Speranza, F., 1999. Magnetic proxy climate results from the Duanjiapo loess section, southernmost extremity of the Chinese loess plateau. J. Geophys. Res. 104B, 645–659.

Forster, T., Evans, M.E., Heller, F., 1994. The frequency of low field susceptibility in loess sediments. Geophys. J. Int. 118, 636–642.

Fukuma, K., Torri, M., 1998. Variable shape of magnetic hysteresis loops in the Chinese loess–paleosol sequences. Earth Planets Space 50, 9–14.

Geiss, C.E., Zanner, C.W., Banerjee, S.K., Joanna, M., 2004. Signature of magnetic enhancement in a loessic soil in Nebraska, United States of America. Earth Planet. Sci. Lett. 228, 355–367.

Guo, Z.T., Biscaye, P., Wei, L.Y., Chen, X.H., Peng, S.Z., Liu, T.S., 2000. Summer monsoon variations over the last 1.2 Ma from the weathering of loess–soil sequences in China. Geophys. Res. Lett. 27, 1751–1754.

Guo, B., Zhu, R.X., Roberts, A.P., Florindo, F., 2001. Lack of correlation between paleoprecipitation and magnetic susceptibility of Chinese loess/paleosol sequences. Geophys. Res. Lett. 28, 4259–4262.

Hao, Q.Z., Guo, Z.T., 2005. Spatial variations of magnetic susceptibility of Chinese loess for the last 600 kyr: implications for monsoon evolution. J. Geophys. Res. 110, B12101. doi:10.1029/2005JB003765.

Heller, F., Liu, T.S., 1984. Magnetism of Chinese loess deposits. Geophys. J. R. Astron. Soc. 77, 125–141.

Heller, F., Liu, T.S., 1986. Paleoclimatic and sedimentary history from magnetic susceptibility of loess in China. Geophys. Res. Lett. 13, 1169–1172.

Heller, F., Shen, C.D., Beer, J., Liu, X.M., Liu, T.S., Bronger, A., Suter, M., Bonani, G., 1993. Quantitative estimates of pedogenic ferromagnetic mineral formation in Chinese loess and palaeoclimatic implications. Earth Planet. Sci. Lett. 114, 385–390.

Huang, J.N., Fang, J.Y., Shao, J.J., 1988. Study on the chronology of Xiashu Loess in Nanjing area. Geological Review 34, 241–246 (in Chinese).

Hunt, C.P., Singer, M.J., Kletetschka, G., TenPas, J., Verosub, K.L., 1995. Effects of citrate–bicarbonate–dithionite treatment on fine-grained magnetite and maghemite. Earth Planet. Sci. Lett. 130, 87–94.

Jahn, B., Gallet, S., Han, J., 2001. Geochemistry of the Xining, Xifeng and Jixian sections, Loess Plateau of China: Eolian dust provenance and paleosol evolution during the last 140 ka. Chem. Geol. 178, 71–94.

Lai, Z.P., Zhou, J., Xia, Y.F., Wang, Y.J., Chen, J., 2001. Luminescence geochronology of Xiashu Loess near Nanjing. J. Desert Res. 21, 116–121 (in Chinese).

Li, L.W., Fang, Y.S., 1993. Research on the Xiashu Loess in Nanjing, China. J. Nanjing Norm. Univ. 16, 3–21 (supplement, (in Chinese)).

Li, X.G., He, J.H., Li, D.S., Li, L.W., 1993. A preliminary study on electron spin resonance dating of the Xiashu Loess. J. Nanjing Norm. Univ. 16 (3), 86–91 (in Chinese).

Li, X.S., Yang, D.Y., Lu, H.Y., 2001. Grain-size features and genesis of the Xiashu Loess in Zhenjiang. Mar. Geol. Quat. Geol. 21, 25–32 (in Chinese).

Liu, T.S., 1985. Loess and the Environment. China Science Press, Beijing (in Chinese).

Liu, X.M., Hesse, P., Rolph, T., 1999. Origin of maghaemite in Chinese loess deposits: Aeolian or pedogenic? Phys. Earth Planet. Inter. 112, 191–201.

Liu, Q.S., Jackson, M.J., Yum, Y.J., Chen, F.H., Deng, C.L., Zhu, R.X., 2004. Grain size distribution of pedogenic magnetic particles in Chinese loess/paleosols. Geophys. Res. Lett. 31, L22603. doi:10.1029/2004GL021090.

Liu, Q.S., Deng, C.L., Torrent, J., Zhu, R.X., 2007. Review of recent developments in mineral magnetism of the Chinese loess. Quat. Sci. Rev. 26, 368–385.

Maher, B.A., 1988. Magnetic properties of some synthetic submicron magnetites. Geophys. J. 94, 83–96.

Maher, B.A., Thompson, R., 1991. Mineral magnetic record of the Chinese loess and paleosols. Geology 19, 3–6.

Maher, B.A., Thompson, R., 1995. Paleorainfall reconstruction from pedogenic susceptibility variations in the Chinese loess and paleosols. Quat. Res. 44, 383–391.

Mehra, O.P., Jackson, M.L., 1958. Iron oxide removal from soils and clays by dithonite–citrate system buffered with sodium bicarbonate. Clays Clay Miner. 7, 317–327.

Mishima, T., Torii, M., Fukusawa, H., Ono, Y., Fang, X.M., Pan, B.T., Li, J.J., 2001. Magnetic grain-size distribution of the enhanced component in the loess–paleosol sequences in the western Loess Plateau of China. Geophys. J. Int. 145, 499–504.

Nesbitt, H.W., Young, G.M., 1982. Early Proterozoic climate and plate motions inferred from major element chemistry of lutites. Nature 299, 715–717.

Qiao, Y.S., Guo, Z.T., Hao, Q.Z., Wu, W.X., Jiang, W.Y., Yuan, B.Y., Zhang, Z.S., Wei, J.J., Zhao, H., 2003. Loess–soil sequences in southern Anhui Province: magnetostratigraphy and paleoclimatic significance. Chin. Sci. Bull. 48, 2088–2093.

Robinson, S.G., Sahota, J.T.S., 2000. Rock-magnetic characterization of early, redoxomorphic diagenesis in turbiditic sediments from the Madeira Abyssal Plain. Sedimentology 47, 367–394.

Sun, X.J., Luo, Y.L., Huang, F., Tian, J., Wang, P.X., 2003. Deep-sea pollen from the South China Sea: Pleistocene indicators of East Asia monsoon. Mar. Geol. 201, 97–118.

Tauxe, L., Mullender, T.A.T., Pick, T., 1996. Potbellies, wasp-waists, and superparamagnetism in magnetite hysteresis. J. Geophys. Res. 101B, 571–583.

Thompson, R., Oldfield, F., 1986. Environmental Magnetism. Allen and Unwin, London.

Verosub, K.L., Fine, P., Singer, M.J., TenPas, J., 1993. Pedogenesis and paleoclimate: interpretation of the magnetic susceptibility record of Chinese loess–paleosol sequences. Geology 21, 1011–1014.

Vidic, N.J., TenPas, J.D., Verosub, K.L., Singer, M.J., 2000. Separation of pedogenic and lithogenic components of magnetic susceptibility in the Chinese loess/paleosol sequence as determined by the CBD procedure and a mixing analysis. Geophys. J. Int. 142, 551–562.

Wei, K.Y., Chiu, T.C., Chen, Y.G., 2003. Toward establishing a maritime proxy record of the East Asian summer monsoons for the late Quaternary. Mar. Geol. 201, 67–79.

Xia, Y.F., Wang, Y.J., Chen, J., 1999. An important stratigraphic boundary in dust accumulation, south China: evidence from magnetic susceptibility. Chin. Sci. Bull. 44, 189–192 (supplement).

Xiao, J.L., An, Z.S., 1999. Three large shifts in East Asian monsoon circulation indicated by loess–paleosol sequences in China and late Cenozoic deposits in Japan. Palaeogeogr. Palaeoclimatol. Palaeoecol. 154, 179–189.

Yang, S.Y., Li, C.X., Yang, D.Y., Li, X.S., 2004. Chemical weathering of the loess deposits in the lower Changjiang Valley China, and paleoclimatic implications. Quat. Int. 117, 27–34.

Yang, S.L., Ding, F., Ding, Z.L., 2006. Pleistocene chemical weathering history of Asian arid and semi-arid regions recorded in loess deposits of China and Tajikistan. Geochim. Cosmochim. Acta 70, 1695–1709.

Zheng, X.M., 1999. Aeolian Deposition and Environment in Changjiang Delta and Extending Sea Areas. East China Normal University Press, Shanghai (in Chinese).

Zheng, H.B., Oldfield, F., Yu, L.Z., Shaw, J., An, Z.S., 1991. The magnetic properties of particle-sized samples from the Luo-Chuan loess section: evidence for pedogenesis. Phys. Earth Planet. Inter. 68, 250–258.

Zhou, L.P., Oldfield, F., Wintle, A.G., Robinson, S.G., Wang, J.T., 1990. Partly pedogenic origin of magnetic variations in Chinese loess. Nature 346, 737–739.